TRAVELING WAVE TUBES

TWT

MPM

MICROWAVE POWER MODULE

TRAVELING-WAVE AMPLIFIERS

VACUUM TUBES

TRAVELING-WAVE TUBE PRINCIPAL COMPONENTS

The TWT possesses four major components as shown in Fig. 1 (1):

1. An electron gun which produces an electron beam
2. A slow-wave circuit which slows an RF electromagnetic wave to a speed synchronous with the electron beam
3. A collector which collects the spent electron beam
4. The TWT package providing cooling, beam focusing, and access to the RF input and output

Amplification is obtained by feeding the RF signal to be amplified into the slow-wave circuit while the electron beam is moving along the TWT axis. The slow-wave structure reduces the electromagnetic wave phase velocity so that it propagates near synchronism with the electron beam resulting in interaction between the wave and the beam, and thus amplification of the RF signal. The spent electron beam is collected at the end of the TWT by the collector.

Electron Gun

The electron gun is used to produce the electron beam. The electron guns used for nearly all TWTs mimic a section of a spherical diode as first derived by Pierce (2), and are consequently referred to as Pierce guns. The major components of the gun are the cathode, heater, focus electrode, and one or more anodes. The type of cathode most commonly used in TWTs is the thermionic cathode where electron emission is achieved by using a heat source to supply the electrons near the surface of the cathode with enough energy to escape from the surface. Cathode operation is a complex subject and the reader can consult (3) or the article on cathodes in this encyclopedia for further detail. In a simplified description, the higher the temperature of the cathode, the greater the emission (current density), but the shorter the life. Because of the limited lifetime of cathodes, the electron gun design must be consistent with the expected life of the application. For example, if a lifetime of 12 to 15 years is required, as in commercial space applications, cathode current densities of 1 A/cm^2 or less are usually specified for an M-type cathode (4).

A heater connected to a dc or ac power supply, consisting of a coil of tungsten or tungsten-rhenium wire adjacent to or embedded within the cathode body is typically used to raise the temperature of the cathode to an adequate level for electron emission. The wire is formed into a contrawound coil to reduce the amount of magnetic field introduced into the electron gun by the current through the heater. This reduces large perturbations in the electron trajectories, which would make the beam difficult to focus or couple modulation onto the electron beam.

The anode is a positively charged electrode which attracts and accelerates the electrons emitted from the cathode. Because of electrostatic repulsion forces, the electrons are deflected as they are emitted so the focus electrode is used to produce equipotential lines with the same center of curvature as the cathode resulting in electron flow toward this center of curvature; therefore, the electrons are focused into a beam. TWTs used in pulsed applications often have a grid placed close to the cathode which permits the electron beam to be turned off and on with a small swing (relative to the cathode-to-ground potential drop) in the applied grid-to-cathode bias. The grid typically causes some perturbation of the electron beam so it is typically not used in high reliability devices.

Non-thermionic cathodes, or field emitter array (FEA) cold-cathodes have been implemented in TWTs with limited success (5, 6). However, the use of FEAs in TWTs is not well-established at this time because of reliability issues.

Slow-Wave Circuit

The RF voltage to be amplified is fed into the slow-wave circuit through the input coupler. The purpose of the slow-wave circuit is to slow down the axial velocity of the RF wave so that it propagates near synchronism with the electron beam. There are numerous possible slow-wave structures. Some of the more common are the helix, contrawound helix, coupled-cavity, ring-bar, cloverleaf, ladder, and grating circuits. The axial component of the electric field set up by the voltage on the circuit is somewhat sinusoidal in the vicinity of the electron beam so a force is directed to the left when the field is positive and to the right when the field is negative (see Fig. 1). This causes some of the electrons in the beam to decelerate (force is directed to the left) and others to accelerate (force is directed to the right), causing the electron beam to form bunches, or be velocity modulated. The bunches drift into a decelerating region of the field and the electrons lose velocity and thus kinetic energy. The energy lost by the electrons is transferred to RF energy in the RF wave, thus amplifying the RF signal. Further down the length of the circuit, the bunches become more compact leaving even more electrons in the decelerating region causing the RF wave to grow even more. As this continues, the electron velocities decrease and space-charge forces within the bunch increase. Eventually a portion of the bunch leaves the decelerating region of the circuit field and enters the accelerating region. These electrons extract energy from the circuit field. When the energy extracted from the circuit field becomes

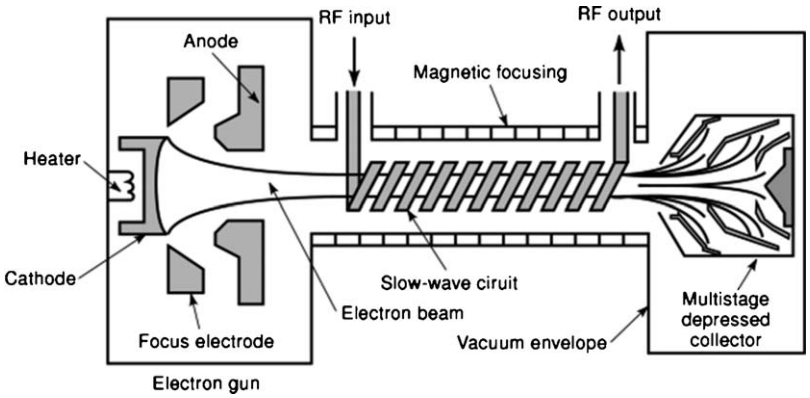

Figure 1. Basic TWT. The electron gun shown to the left encompasses the heater, cathode, focus electrode and anode. A multistage depressed collector is shown on the right with electron beam trajectories.

equal to the energy supplied, amplification of the RF wave stops and the interaction is said to reach saturation.

Backward wave oscillations (*BWO*s) can occur when power is reflected back to the input because of a mismatch in the slow-wave circuit, at the load or at the output coupler. Because of a mismatch at the input, a portion of the signal is again reflected to provide a feedback signal. To prevent these reflections, or backward waves, from reaching the input, it is common that a sever or distributed loss is added to the slow-wave circuit. A sever isolates the input wave from the output wave by physically separating the sections. Distributed loss usually consists of a lossy resistive coating which attenuates both forward and backward waves. Although the RF wave is severed or attenuated at this point in the slow-wave circuit, the bunching of the electrons has been established and will reestablish the RF wave on the circuit beyond the sever or region of attenuation, allowing interaction to continue.

A common method to increase efficiency by prolonging synchronism between the electron beam and the RF wave is to incorporate a velocity taper in the TWT design. A velocity taper is achieved by changing the dimensions of the slow-wave circuit near the output of the tube so that the RF wave velocity is slowed along with the electron beam. With this technique, even though the electron bunches are slowed as they lose energy to the circuit, they will remain in synchronism longer with the consecutively slowed RF wave and continue to deliver energy to the circuit fields. Velocity tapering has proved to significantly increase the efficiency of TWTs (7–9). In addition, the technique can be used to enhance the linearity of the power output versus power input (10, 9) and to prevent BWOs (11–13).

Helix. The helix is the most common type of slow-wave structure. A typical modern helical structure embodies a metal tape wound into a helix supported by three or more dielectric support rods inside a conducting barrel. Figure 2 shows the cross-sectional view of a typical helical circuit and a three-dimensional view of the helical tape. Derived from a single-wire transmission line which has zero dispersion, the helix has a primarily constant phase velocity over a large bandwidth making it the widest bandwidth circuit of any structure available. This relatively low dispersion can be reduced further by incorporating dispersion shaping techniques into the circuit design. This is achieved by perturbing the circuit fields predominantly at low frequencies

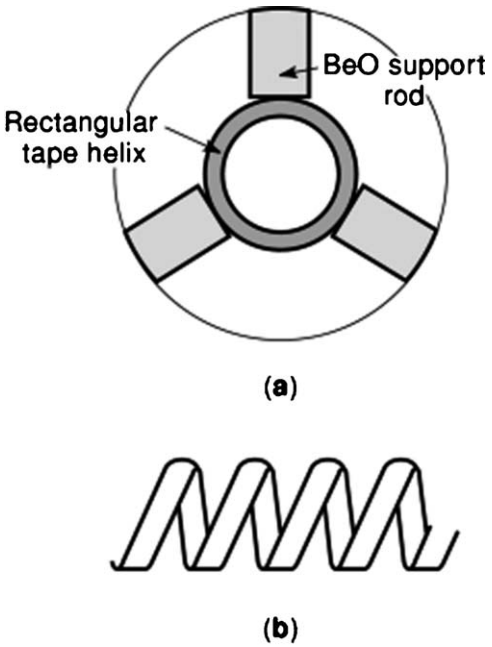

Figure 2. Cross-sectional view of typical helix slow-wave circuit and three-dimensional view of helical tape. The rectangular helical tape is supported by three rectangular dielectric support rods, all enclosed in a conducting barrel. The electron beam travels through the axial center (r = 0) of the helical circuit.

so that the phase velocity is decreased at the low frequency end while staying constant at high frequencies, thus reducing dispersion and increasing bandwidth. Since the fields are concentrated between the helical turns at high frequencies and in the area extending from the helix to the barrel at low frequencies, this low frequency perturbation is possible by including specially shaped dielectric support rods or longitudinally conducting metal vanes which anisotropically load the circuit (3, 14). Several loading methods are shown in Fig. 3.

Coupled-Cavity Circuit. Another common slow-wave structure is the coupled-cavity circuit which is used mostly for high-power applications. Because of its all metal construction, it is able to dissipate a greater amount of heat compared to the helix, but can operate over only a comparatively narrow bandwidth. As shown in Fig. 4 for the

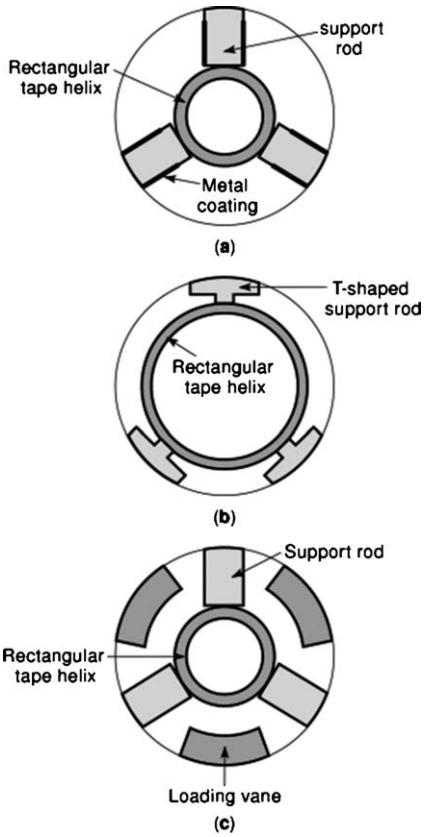

Figure 3. Various dispersion shaping techniques for broadband helical TWTs. (a) A metal coating is applied to the dielectric support rods. (b) The support rods are formed into T-shapes. (c) Loading vanes are added between the support rods.

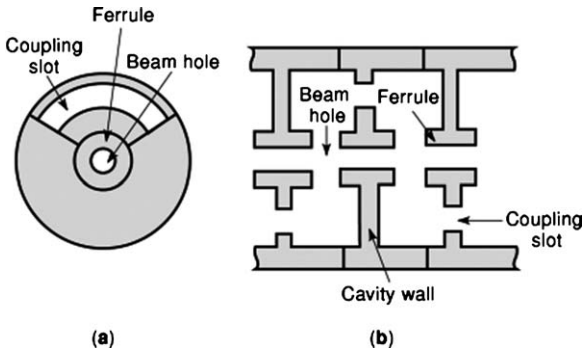

Figure 4. (a) Cross-sectional view, (b) top view of ferruled coupled-cavity circuit. The coupled cavity circuit employs an all-metal construction suitable for high-power TWTs.

cross-sectional and top views, the circuit includes a chain of cavities, typically made of copper, brazed together with a coupling slot alternating 180 degrees at adjacent cavities. Ferrules may surround the beam hole to concentrate the RF electric field in the vicinity of the electron beam for increased interaction.

Collector

After the amplified RF output is removed from the TWT the spent electron beam passes through the end of the beam focusing section, so space charge forces cause the beam to expand as it enters the collector. Upon entering the collector, the beam is highly disordered with a broad spectrum of energies. The electron beam at this point still possesses a great deal of kinetic energy as only about 5 to 30 percent is extracted during interaction with the RF wave (15). If the collector were at the same potential as the body of the tube, this kinetic energy would be dissipated as heat on the collector surface. By operating the collector electrode at a potential below that of the RF circuit, the beam is decelerated before it hits the collector surface. Thus, some of the remaining kinetic energy from the electron beam is converted to electric potential energy. This negative potential operation is known as depressing the collector. The greater the amount of recovered power, the higher the total efficiency of the tube. The impact of an efficient collector is made clear by considering the efficiency formula. Overall efficiency can be expressed as the ratio of the output power to input power or

$$\eta_{0v} = \frac{P_{out}}{P_{in}} \qquad (1)$$

where P_{out} is the RF power output and P_{in} is the sum of the heater power, P_h, beam power from the gun, P_o, RF input power, P_{RFin}, and power to the magnetic focusing system, P_m, minus the power recovered by the collector, P_{rec}, or

$$P_{in} = P_h + P_o + P_m + P_{RFin} - P_{rec} \qquad (2)$$

Figure 5(a) plots the current to the collector versus the amount by which the collector is depressed below ground potential (the slow-wave circuit potential). Assuming zero loss and zero interception between the beam and the slow-wave circuit, the area under the curve represents the maximum power that could possibly be recovered by the collector. The beam power converted to RF power is represented by the area above the curve less the cross-hatched area for voltages greater than the beam voltage. The beam current and voltage are represented by I_o and V_o, respectively. For a single stage collector depressed to voltage V_1, the maximum power that can be recovered is represented graphically in Fig. 5(a) by the shaded area which is the product of the magnitudes of the collector current and collector voltage or

$$P_{rec} = V_1 I_o$$

Several phenomena complicate the collector operation including space-charge effects of the electrons already in the collector repelling those electrons entering, secondary electron emission from the surface caused by incident electrons, and electrons having different amounts of kinetic energy, thus traveling with different velocities. Multistage depressed collectors (*MDC*), where several electrodes are used at different depressed potentials, incorporate multiple velocity sorting stages. This directs high velocity electrons to the stages having the greatest depression and the slow electrons to the stages with the least depression. This design has proven to greatly increase the overall efficiency of TWTs (16). The reason for this becomes clear when the collector current versus voltage curve is again considered for the multistage collector. The total possible recoverable

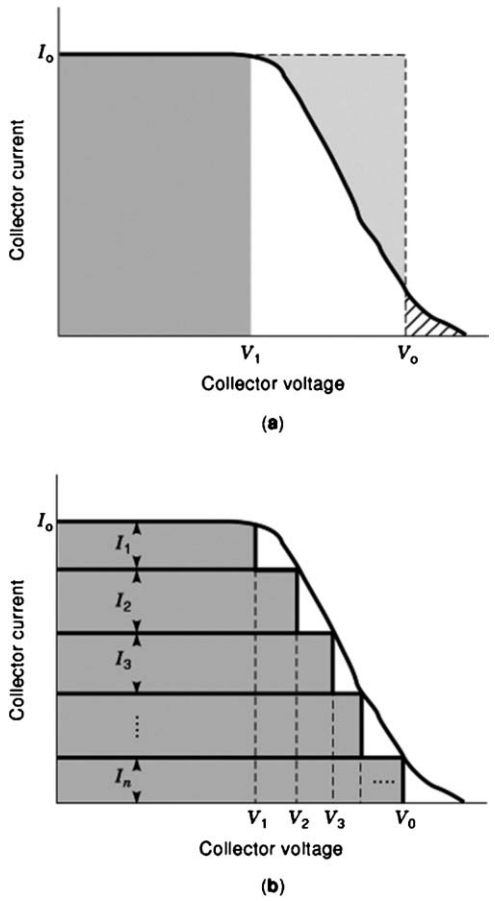

Figure 5. Collector current versus collector voltage. (a) The dark shaded area designates the maximum power which can be recovered by a single-stage collector. (b) The dark shaded area designates the maximum power which can be recovered by a multistage depressed collector with n stages.

power for an n-stage MDC is represented by the shaded region in Fig. 5(b) where the nth electrode is at cathode potential, V_o. The possible recovered power is significantly greater compared to the single stage collector given as

$$P_{\text{rec}} = \sum_{k=1}^{n} V_k I_k$$

In practice this can never be exactly achieved because of secondary emission and imperfect energy sorting in the collector. Considering Eqs. (1) and (2), it becomes obvious that the overall efficiency can be significantly increased. In practice, typical MDC designs incorporate no more than five collector stages as the law of diminishing returns starts to occur with regard to efficiency improvement versus fabrication and power supply complexity. A typical azimuthally symmetric four-stage MDC design is shown in two dimensions in Fig. 1.

Traveling-Wave Tube Package

The TWT package serves as a mechanical support structure for the TWT and RF input/output connectors, a thermal path for the conduction of waste heat, an electromagnetic interference (*EMI*) shield and as a protective cover

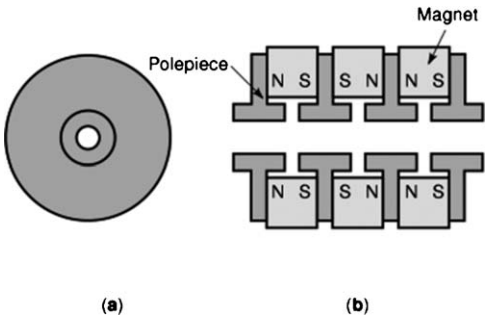

Figure 6. (a) Cross-sectional view, (b) top view of periodic permanent magnet focusing.

over the high voltage connections and beam focusing magnets (17).

Beam Focusing. The electrons in the beam each possess negative charge; therefore, they repel one another causing the beam to diverge. To counteract this space charge effect and prevent the beam from diverging and being intercepted by the slow-wave structure as it flows through the length of the tube, external focusing is applied, most commonly using an axial magnetic field. One way of doing this is to surround the TWT with a large solenoid which can be a permanent magnet or an electromagnet. Because of their size and large amount of stray magnetic field, solenoids are typically used only on very high power (kilowatt level) TWTs with high current density beams.

A more commonly used method for focusing is to employ periodic permanent magnet (*PPM*) focusing which is lighter and more compact than an equivalent solenoidal magnet (18). Alternating iron pole pieces and cylindrical magnets are placed side-by-side along the length of the tube, the polarity of adjacent magnets being reversed, as shown in Fig. 6. The PPM structure provides a nearly sinusoidal magnetic field at the beam axis with *rms* (root-mean-square) value about equal to the value of field required in a uniform field design.

Although not as common, electrostatic focusing is an alternative to magnetic focusing schemes. If compatible with the application, electrostatic focusing can offer a relatively lower cost and lower mass alternative to magnetic focusing (19, 20).

Vacuum Envelope. It is necessary to operate the main components of the TWT under vacuum to ensure proper cathode operation and long cathode life, prevent formation of positive ions within the electron beam, and to avoid high voltage arcing at the electrodes. Thus, the gun, slow-wave structure, and collector are contained in a leak tight vacuum envelope. The beam focusing mechanism is usually mounted outside of the vacuum envelope and this whole assembly is mounted in the TWT package.

BASIC FIELD THEORY

TWT gain is based on the surrender of energy from the electron beam to the RF electromagnetic wave. For this phenomena to occur the phase velocity of the RF wave,[1] v,

must be in near synchronism with the dc beam velocity, u_o, or

$$v = u_o \tag{3}$$

The gain of the TWT depends on the strength of this interaction. A summary of the small-signal analysis for TWT gain is summarized by Gilmour (3), Gewartowski (21) and more succinctly by Wilson (22), based on the analysis done by Pierce (23). The theory neglects space harmonics of the RF field other than that which is synchronous with the electron beam assuming these harmonics have no net effect.

First, the equation is derived for the ac current induced on the beam by the RF field (electronic equation). Next, the RF field resulting from the modulated beam is derived (circuit equation). These equations are solved simultaneously to determine the self-consistent relations for the circuit and beam quantities. The equations take on a neater form when several parameters are defined. Pierce's small-signal gain parameter C is defined as

$$C^3 = \frac{KI_o}{4V_o} \tag{4}$$

where K is the average interaction impedance over the beam cross section defined as

$$K = \frac{\int |E|^2 dS}{2\beta^2 PS} \tag{5}$$

where $|E|$ is the magnitude of the RF axial electric field, $\beta = \omega/\mu$ is the axial propagation constant,[2] P is the total RF power flow and S is the cross-sectional surface area of the electron beam. I_o and V_o are the dc beam current and voltage, respectively. Pierce's space-charge parameter QC is defined as

$$\mathrm{QC} = \frac{\omega_q^2}{4C^2\omega^2} \tag{6}$$

where ω_q is the reduced plasma frequency and ω is the angular frequency ($2\pi f$), where f is the operating frequency.

A measure of synchronism between the electrons and the space harmonic wave is specified by Pierce's velocity parameter b defined as

$$b = \frac{u_o - v}{vC} = \frac{b_0 - N}{NC} \tag{7}$$

Pierce's loss parameter d is proportional to circuit attenuation and is defined as

$$d = \frac{\alpha\omega}{u_o C} \tag{8}$$

where α is the circuit attenuation including surface and attenuator losses. The various fields and beam quantities have a z dependence of the form

$$e^{-\Gamma z}$$

where Γ is the complex propagation constant for the circuit-beam coupled system. The allowed values for Γ are determined by simultaneously solving for the circuit and electronic equations. Doing so gives

$$\Gamma = j\frac{u_o}{\omega}(1 + jC\delta) \tag{9}$$

Making the appropriate substitutions and taking advantage of the fact that C is small,

$$\delta^2 = \frac{1}{-b + jd + j\delta} - 4QC \tag{10}$$

The solutions for Eq. (13) give three allowable propagation constants. Regardless of the values of d and QC, one will always obtain one growing wave which is responsible for the gain in the tube, one decaying wave, and one wave of nearly constant amplitude as long as the tube is operating near synchronism (small b).

The initial loss factor A_1 is defined as

$$A_1 = 20\log\left|\frac{\delta_1^2}{(\delta_1 - \delta_2)(\delta_1 - \delta_3)}\right| \mathrm{dB} \tag{11}$$

The space-charge loss factor is defined as

$$A_2 = 20\log\left|\frac{\delta_1^2 + 4QC}{\delta_1^2}\right| \mathrm{dB} \tag{12}$$

Next we define

$$B = 54.6\mathrm{Re}(\delta_1) \tag{13}$$

and the electronic wavelength number N as

$$N = \frac{u_o l}{2\pi\omega} \tag{14}$$

where l is the length of the interaction circuit. The small-signal gain can now be expressed as

$$\mathrm{Gain}_{s-s} = A_1 + A_2 + BCN - \text{sever loss dB} \tag{15}$$

The loss associated with each sever is typically about 6 dB. It should be noted that the small-signal gain analysis is valid only when the tube is operating well below saturation. Near or at saturation, the TWT behaves in a nonlinear manner and the small-signal theory is no longer valid.

TRAVELING-WAVE TUBE COMPUTER MODELING

Because of the complexity of operation, there are numerous codes which are used in the design, development, and analysis of TWTs. A discussion of some of the available codes follows which is grouped by TWT section. This is intended to point the reader to appropriate references for each code.

Electron Gun. Numerous codes exist which will calculate electron trajectories in electrostatic and magnetostatic focusing systems. Electron gun (*EGUN*) is a widely used code which includes two-dimensional (2-D) fields and three-dimensional (3-D) particle trajectories (24). In contrast to EGUN's rectangular mesh capability, DEMEOS uses a deformable triangular mesh which is efficient in modeling both the small and relatively large dimensions of the electron gun (25). Trak and OmniTrak are 2-D and 3-D finite element codes, respectively, that calculate single-particle orbits or simulate steady-state beams (planar or cylindrical), electric and magnetic fields (26). The 3-D particle-in-cell (*PIC*) code MAGIC is also used in gun

design (27). Additional codes used for electron gun design include Beam Optics Analysis (BOA) (28, 29), MICHELLE (30, 31), MAFIA (32), and Particle Studio (32).

Slow-Wave Structure

There is a large variety of codes available for the analysis of slow-wave structures. An important step in TWT design is to obtain the cold-test characteristics of the circuit. Cold-testing implies testing the circuit or a scale model of the circuit on the RF test bench without the electron beam to obtain dispersion, interaction impedance, and attenuation characteristics. Accurate results have been obtained in terms of cold-test parameters for several slow-wave circuits using codes like MAFIA (33, 34), High Frequency Structure Simulator (HFSS) (35), Microwave Studio (MWS) (32), CUTLSS (36), the 3-D cold-test code for helical structures TLM (37) and the 3-D cold-test code limited to axially symmetric cavities in cylindrical coordinates SUPERFISH (38).

It is also important to obtain information about the match from the slow-wave structure to the input/output couplers. Accurate results regarding the transmission characteristics of TWT couplers have been obtained using codes like Cascade (39), HFSS, MWS, and MAFIA.

Collector

There has been significant progress made in the computational modeling of collectors within the past several years. Typically an electron trajectory code such as EGUN was used to aid in collector design (40), but because it can simulate only azimuthally symmetric structures with steady-state electron streams, three-dimensional codes that compute instantaneous conditions are also being used. Several 3-D codes have provided reasonably accurate results: the 3-D PIC code, MAFIA (41); C3D (42); the 3-D PIC code, PIC3D (43), the 3-D electron trajectory collector simulator, LKOBRA (44), BOA (28), and MICHELLE (31).

Traveling-Wave Tube Interaction

As mentioned previously, the field theory for small-signal gain provides insight into TWT interaction, but when the tube is operated near or at saturation, this analysis is no longer valid. Near saturation the TWT behaves in a nonlinear manner referred to as large-signal operation. This means that when large-amplitude signals are present, higher order RF terms are no longer negligible as compared to the corresponding dc values. The analysis of the nonlinear system does not lend itself to neat solutions of closed form equations, so computational modeling becomes crucial (45). There are a number of codes available to simulate TWT interaction and thus provide characteristics such as gain, power transfer curves, and efficiency near and at saturation.

There are several codes devoted strictly to helical TWT interaction such as the one-dimensional (1-D) and 3-D codes which predict intermodulation distortion, CHRISTINE (9) and CHRISTINE 3-D (46), respectively, the 2-D code which incorporates 3-D field vector components and beam velocities GATOR (47), the 2-D code, TWA3 (48), and the 2-D deformable disk model DDM HELIX TWT (49). The NASA CC TWT code analyzes interaction between a 3-D electron beam and 2-D RF electromagnetic fields in coupled-cavity TWTs (50). Fully three-dimensional PIC codes such as MAFIA, 3DPIC and MAGIC offer the advantage of being able to simulate an entire TWT section in 3-D including modulation effects. Modeling the beam dynamics in just the TWT slow-wave section in 3-D has been accomplished with good accuracy (51–53) but an entire 3-D TWT model from gun to collector has not yet been accomplished because of the computational intensity of the problem.

FUTURE TRENDS

The microwave power module (*MPM*) is a fairly recent development which has had a significant impact on microwave and millimeter-wave electronics system development by taking advantage of the best features of both vacuum electronics and solid-state devices. The MPM is a lightweight, miniaturized RF amplifier consisting of a low noise, high-gain microwave monolithic integrated circuit (*MMIC*) preamplifier/signal conditioner, a high efficiency vacuum power booster TWT, and a miniaturized high efficiency integrated power conditioner. The MPM has proven to outperform conventional TWT technology in areas of power density (power per unit weight) and noise figure. Analyses also indicate improvement in reliability due to fewer components, lower typical operating temperatures, and improved interconnection technology (54).

Micro-fabrication is becoming an integral part of higher frequency (greater than ∼60 GHz) TWTs. Because of the small size of the components, conventional fabrication techniques become very expensive and difficult, if not impossible, to use. Thus, applied fabrication techniques include deep reactive ion etching (DRIE), laser ablation, LIGA (German acronym for X-ray lithography (X-ray Lithographie), Electroplating (Galvanoformung), and Molding (Abformung)), and micro-EDMing. Integrating these processes into TWT fabrication promises very high frequency operation into the THz regime (55–61).

BIBLIOGRAPHY

1. R. Kompfner The invention of the traveling-wave tubes, *IEEE Trans. Electron Devices*, **ED-23**: pp. 730–738, 1976.
2. J. R. Pierce *Theory and Design of Electron Guns*, Second ed. New York: Van Nostrand, 1954.
3. A. S. Gilmour, Jr. *Principles of Traveling-Wave Tubes.* Norwood, MA: Artech House, 1994, pp. 328–329.
4. J. A. Dayton, Jr.Traveling-wave tube amplifier reliability, 1995 IEEE MTT-S International Microwave Symposium/TWTA Workshop Proc., May 1995.
5. K. L. Jensen, Field emitter arrays for plasma and microwave source applications, *Physics of Plasmas*, Volume**6**, Issue 5, pp. 2241–2253, 1999.

* The RF wave actually consists of space harmonics and the harmonic component of interest must be near synchronism with the dc beam velocity.

† K, E, and β are calculated for the space harmonic of interest.

6. D. R. Whaley, B. M. Gannon, C. R. Smith, C. M. Armstrong, C. A. Spindt, Application of field emitter arrays to microwave power amplifiers, *IEEE Trans. Plasma Science*, Volume**28**, Issue 3, pp. 727–747, 2000.
7. A. N. Curren, R. W. Palmer, D. A. Force, L. Dombro, J. A. Long, High-efficiency helical traveling-wave tube with dynamic velocity taper and advanced multistage depressed collector, IEEE Int. Electron Devices Meet. Tech. Dig., pp. 473–476, 1987.
8. J. D. Wilson, H. C. Limburg, J. A. Davis, I. Tammaru, J. P. Vaszari, A high efficiency ferruleless coupled-cavity traveling-wave tube with phase-adjusted taper. *IEEE Trans. Electron Devices*, **ED-37**: pp. 2638–2643, 1990.
9. D. K. Abe, B. Levush, T. M. Antonsen, Jr. D. R. Whaley, B. G. Danly, Design of a linear C-band helix TWT for digital communications experiments using the CHRISTINE suite of large-signal codes, *IEEE Trans. Plasma Science*, Volume**30**, Issue 3, Part 1, pp. 1053–1062, 2002.
10. H. G. Kosmahl and J. C. Peterson, A TWT amplifier with a linear power transfer characteristic and improved efficiency, NASA TM-83590, March 1984.
11. G. I. Haddad and R. M. Bevensee, Start-oscillation conditions of tapered backward-wave oscillators, *IEEE Trans. Electron Devices*, **ED-10**: pp. 389–393, 1963.
12. B. Epsztein and G. Kantrowicz, Suppression of backward-wave oscillations in multikilowatt helix TWT's, Proc. European Microwave Conf., pp. 376–380, September 1973.
13. K. Tsutaki, Y. Yuasa, and Y. Morizumi, Numerical analysis and design for high-performance helix traveling-wave tubes, *IEEE Trans. Electron Devices*, **ED-32**: pp. 1842–1849, 1985.
14. J. L. Putz and M. J. Cascone, Effective use of dispersion shaping in broadband helix TWT circuits, IEEE Int. Electron Devices Meet. Tech. Dig., pp. 422–424, 1979.
15. J. W. Hansen, System Aspects of Communications TWTA's, Hughes Aircraft Company Electron Dynamics Division Applications Note, 1983.
16. H. G. Kosmahl, Modern multistage depressed collectors—A review, *Proc. IEEE Trans. Electron Devices*, **ED-70**: pp. 1325–1334, 1982.
17. TWT/TWTA Handbook, Hughes Aircraft Company, Electron Dynamics Division, Torrance, CA, 1992.
18. J. T. Mendel, C. F. Quate and W. H. Yocom, Electron beam focusing with periodic permanent magnet fields, *Proc. IRE*, pp. 800–810, May 1954.
19. E. F. Belohoubek, W. W. Siekanowicz and F. E. Vaccaro, Design and performance of an electrostatically focused 5-kw X-band traveling-wave tube, *IEEE Trans. Electron Devices*, Volume**11**, Issue 3, pp. 102–114, 1964.
20. B. K. Vancil and E. G. Wintucky, A low cost electrostatically focused TWT, Third IEEE International Vacuum Electronics Conference, pp. 180–181, 2002.
21. J. W. Gewartowski and H. A. Watson *Principles of Electron Tubes.* New Jersey: D. Van Nostrand, 1965, pp. 349–370.
22. J. D. Wilson, Traveling-wave thermionic devices. InT. Koryu Ishii's *Handbook of Microwave Technology, Volume 2*, San Diego: Academic Press, 1995, pp. 57–95.
23. J. R. Pierce *Traveling-Wave Tubes*, New York: Van Nostrand, 1950, pp. 5–18.
24. W. B. Herrmannsfeldt, Electron trajectory program, *Stanford Linear Accelerator Center Rep. 331*, Stanford Univ., Stanford, CA, 1988.
25. R. True, Electron beam formation, focusing, and collection in microwave tubes, inT. Koryu Ishii's *Handbook of Microwave Technology*, Vol. 1, San Diego: Academic Press, 1995, pp. 497–567.
26. http://www.fieldp.com/index.html
27. K. Nguyen, G. D. Warren, L. Ludeking and B. Goplen, Analysis of the 425-MHz klystrode, *IEEE Trans. Electron Devices*, **ED-38**: pp. 2212–2220, 1991.
28. http://calcreek.com/downloads/BOAManual.pdf#search=%22electron%20gun%20BOA%22
29. B. M. Lewis, H. T. Tran, M. E. Read, R. L. Ives, Design of an electron gun using computer optimization, *IEEE Trans. Plasma Science*, Volume**32**, Issue 3, Part 1, pp. 1242–1250, June 2004.
30. http://www.saic.com/products/software/michelle/
31. J. Petillo, K. Eppley, D. Panagos, P. Blanchard, E. Nelson, N. Dionne, J. DeFord, B. Held, L. Chernyakova, W. Krueger, S. Humphries, T. McClure, A. Mondelli, J. Burdette, M. Cattelino, R. True, K. T. Nguyen and B. Levush, The MICHELLE three-dimensional electron gun and collector modeling tool: theory and design, *IEEE Trans. Plasma Science*, Volume**30**, Issue 3, Part 1, pp. 1238–1264, June 2002.
32. http://www.cst.com/
33. C. L. Kory and J. D. Wilson, Three-dimensional simulation of traveling-wave tube cold-test characteristics using MAFIA, NASA TP-3513, May 1995.
34. C. L. Kory, J. D. Wilson, and J. W. Maruschek, Simulation of cold-test dispersion and interaction impedance for coupled-cavity traveling-wave tube slow-wave circuits, IEEE Int. Electron Devices Meet. Tech. Dig., pp. 763–766, 1992.
35. http://www.ansoft.com/products/hf/hfss/index.cfm?&vflash=y
36. S. J. Cooke, A. Mondelli, B. Levush, T. M. Antonsen, Jr, D. P. Chernin, T. H. McClure, D. R. Whaley and M. Basten, CTLSS-an advanced electromagnetic simulation tool for designing high-power microwave sources, *IEEE Trans. Plasma Science*, Volume**28**, Issue 3, pp. 841–866, June 2000.
37. K. D. Ward and J. Wlodarczyk, Transmission line modeling of helix slow-wave structures, *IEEE Int. Electron Devices Meet. Tech. Dig.*, pp. 157–160, 1993.
38. K. Halbach and R. F. Holsinger, Superfish—A computer program for evaluation of RF cavities with cylindrical symmetry, *Part. Accel.*, **7**: pp. 213–222, 1976.
39. http://calcreek.com/cascade.html
40. J. A. Dayton, Jr. *et al.*Analytical prediction with multidimensional computer programs and experimental verification of the performance, at a variety of operating conditions, of two traveling-wave tubes with depressed collectors, NASA TP-1449, May 1979.
41. K. R. Vaden, V. O. Heinen and J. A. Dayton, Jr. Three dimensional modeling of multistage depressed collectors, Proc. IEEE Int. Conf. on Plasma Science (ICOPS), 198, 1997.
42. L. Ludeking and J. Geary, C3D, A three-dimensional tool for collector design, Proc. 1996 Microwave Power-Tube Conference, May 1996.
43. K. D. Ward, M. J. Duffield and A. R. Wise, Power-booster traveling-wave tubes, Proc. Microwave Tubes for Space, Military and Commercial Applications Workshop, Noordwijk, The Netherlands, April 1997.
44. L. Kumar *et al.* Three-dimensional simulation of multistage depressed collectors on micro-computers, *IEEE Trans. Electron Devices*, **42**: pp. 1663–1673, 1995.
45. J. E. Rowe, *Nonlinear Electron-Wave Interaction Phenomena*, New York: Academic Press, 1965.

46. D. Chernin, T. M. Antonsen, Jr, B. Levush, and D. Whaley, CHRISTINE 3D: a 3D multi-frequency large signal simulation code for helix traveling wave tubes, 2000 International Vacuum Electronics Conference Proceedings, May 2-4, 2000.
47. H. P. Freund and E. G. Zaidman, GATOR: A 3D time-dependent simulation code for helix TWT's, Proc. IEEE Int. Conference on Plasma Science (ICOPS), 197, 1997.
48. D. M. MacGregor, Two-dimensional nonlinear multisignal helix traveling-wave tube amplifier computer program, Volume 1: User Manual, Electrocon International, Inc., Ann Arbor, Michigan, April 1993.
49. H. K. Detweiler, Characteristics of magnetically focused large-signal traveling-wave amplifiers, Rome Air Development Center Tech. Rep. RADC-TR-68-433, Griffiss Air Force Base, NY, 1968.
50. J. D. Wilson, Revised NASA axially symmetric ring model for coupled-cavity traveling-wave tubes, NASA TP-2675, 1987.
51. K. D. Ward, M. J. Duffield and A. R. Wise, Power-booster traveling-wave tubes, Proc. Microwave Tubes for Space, Military and Commercial Applications Workshop, Noordwijk, The Netherlands, April 1997.
52. F. Friedlander *et al.*, Transient analysis of beam interaction with antisymmetric mode in truncated periodic structure using three-dimensional computer code "SOS", *IEEE Trans. Electron Devices*, **ED-33**: pp. 1896–1901, 1986.
53. C. L. Kory, Investigation of fully three-dimensional helical RF field effects on TWT beam/circuit interaction, *IEEE Trans. Electron Devices*, Volume**48**, Issue 8, pp. 1718–1726, Aug. 2001.
54. C. Smith *et al.*, MPM technology—The miniaturized transmitter solution.Proc. Microwave Tubes for Space, Military and Commercial Applications Workshop, Noordwijk, The Netherlands, April 1997.
55. R. L. Ives, Development of Microfabricated Traveling Wave Tubes, *IEEE Trans. Plasma Science*, Vol.**32**, No. 3, June 2004.
56. C. Kory, R. L. Ives, M. Read, J. Booske, H. Jiang, D. van der Weide, and P. Phillips, Microfabricated W-band traveling wave tubes, The Joint 30th International Conference on Infrared and Millimeter Waves and 13th International Conference on Terahertz Electronics, 2005, Volume 1, pp. 85–86, Sept. 19-23, 2005.
57. S. Bhattacharjee, J. H. Booske, C. L. Kory, D. van der Weide, S. Limbach, S. Gallagher, J. D. Welter, M. R. Lopez, R. M. Gilgenbach, R. L. Ives, M. E. Read, R. Divan, D. C. Mancini, Folded waveguide traveling-wave tube sources for terahertz radiation, *IEEE Trans. Plasma Science*, Volume**32**, Issue 3, Part 1, 1002–1014, June 2004.
58. L. Lei, and W. Gao, W-band MEMS TWT- array, Infrared and Millimeter Waves, 2004 and 12th International Conference on Terahertz Electronics, 2004.Conference Digest of the 2004 Joint 29th International Conference on 27 Sept.-1, pp. 681–682, Oct. 2004.
59. Seong-Tae Han; K. H. Jang, Jin-Kyu So, Jung-Il Kim, Young-Min Shin, N. M. Ryskin, Chang Suk-Sang, Gun-Sik Park, Low-voltage operation of Ka-band folded waveguide traveling-wave tube, *IEEE Trans. Plasma Science*, Volume**32**, Issue 1, Part 1, pp. 60–66, Feb. 2004.
60. Young-Min Shin, Gun-Sik Park, G. P. Scheitrum, B. Arfin, Novel coupled-cavity TWT structure using two-step LIGA fabrication, *IEEE Trans. Plasma Science*, Volume**31**, Issue 6, Part 2, pp. 1317–1324, Dec. 2003.
61. J. A. Dayton, Jr., G. T. Mearini, Hsiung Chen, C. L. Kory, Diamond-studded helical traveling wave tube, *IEEE Trans. Electron Devices*, Volume**52**, Issue 5, pp. 695–701, May 2005.

CAROL L. KORY
ANALEX Corporation,
Cleveland, OH